

Article

High Performance of Titanium Dioxide Reinforced Acrylonitrile Butadiene Rubber Composites

Wannarat Chueangchayaphan, Piyawadee Luangchuang and Narong Chueangchayaphan *

Faculty of Science and Industrial Technology, Prince of Songkla University, Surat Thani Campus, Surat Thani 84000, Thailand

* Correspondence: narong.c@psu.ac.th

Abstract: Recently, dielectric elastomer actuators (DEA) have emerged as one of the most promising materials for use in soft robots. However, DEA needs a high operating voltage and high mechanical properties. By increasing the dielectric constant of elastomeric materials, it is possible to decrease the operating voltage required. Thus, elastomeric composites with a high dielectric constant and strong mechanical properties are of interest. The aim of this research was to investigate the effect of titanium dioxide (TiO_2) content ranging from 0 to 110 phr on the cure characteristics, and physical, dielectric, dynamic mechanical, and morphological properties of acrylonitrile butadiene rubber (NBR) composites. The addition of TiO_2 reduced the scorch time (t_{s1}) as well as the optimum cure time (t_{c90}) but increased the cure rate index (CRI), minimum torque (M_L), maximum torque (M_H), and delta torque ($M_H - M_L$). The optimal TiO_2 content for maximum tensile strength and elongation at break was 90 phr. Tensile strength and elongation at break were increased by 144.8% and 40.1%, respectively, over pure NBR. A significant mechanical property improvement was observed for TiO_2 -filled composites due to the good dispersion of TiO_2 in the NBR matrix, which was confirmed by scanning electron microscopy (SEM). Moreover, incorporating TiO_2 filler gave a higher storage modulus, a shift in glass transition temperature (T_g) to a higher temperature, and reduced damping in dynamic mechanical thermal analysis (DMTA). The addition of TiO_2 to NBR rubber increased the dielectric constant of the resultant composites in the tested frequency range from 10^2 to 10^5 Hz. As a result, TiO_2 -filled NBR composite has a high potential for dielectric elastomer actuator applications.

Keywords: acrylonitrile butadiene rubber; titanium dioxide; mechanical properties; dielectric properties



Citation: Chueangchayaphan, W.; Luangchuang, P.; Chueangchayaphan, N. High Performance of Titanium Dioxide Reinforced Acrylonitrile Butadiene Rubber Composites. *Polymers* **2022**, *14*, 5267. <https://doi.org/10.3390/polym14235267>

Academic Editors: Dong Yu Zhu, Yingchun Liu and Maoping Lu

Received: 19 October 2022

Accepted: 30 November 2022

Published: 2 December 2022

Publisher's Note: MDPI stays neutral with regard to jurisdictional claims in published maps and institutional affiliations.



Copyright: © 2022 by the authors. Licensee MDPI, Basel, Switzerland. This article is an open access article distributed under the terms and conditions of the Creative Commons Attribution (CC BY) license (<https://creativecommons.org/licenses/by/4.0/>).

1. Introduction

Dielectric elastomer actuators (DEA) are a class of electroactive polymers that deform when an electric field is applied. It can exhibit large deformation, fast response, and high energy density under the external electrical field. DEA can be used in several applications, including electric-induced actuators, soft robotic structures, and smart electronic skins [1,2]. In order to induce deformation, DEA requires a high operating voltage (several kilovolts), which limits its commercial viability. However, the required operating voltage can be reduced by increasing the energy density of the elastomer, which can be achieved by decreasing the thickness of the dielectric elastomer or increasing the dielectric constant of elastomeric materials [1,3]. A conventional method for enhancing the dielectric constant of an elastomer involves inserting dipole groups into the rubber chain or incorporating a filler with a high dielectric constant [3,4].

Acrylonitrile butadiene rubber (NBR) is a copolymer of acrylonitrile and butadiene monomers. Due to acrylonitrile having a functional group ($\text{C}\equiv\text{N}$), NBR presents a specialty polar rubber with a high dielectric constant. NBR has been extensively used as a workhorse in industrial and automotive rubber products [5] because it has beneficial properties such as a broad temperature application range, bonding performance, excellent oil and solvent resistance, and relatively low cost [6,7]. However, NBR does not exhibit self-reinforcing

behaviors [8], as there is no strain-induced crystallization due to its irregular molecular structure of random copolymers, resulting in comparatively weak mechanical properties [9]. Thus, efforts have to be directed at finding an appropriate filler for NBR to achieve high-performance products with good mechanical properties. Several fillers, namely clay [10–12], carbon black [13–16], carbon nanotubes [16–18], and silica [16,19–21]; have been tested for NBR.

Fillers aim to reduce cost and improve mechanical, thermal, and electrical properties. Titanium dioxide (TiO_2) has been attractive because of its great characteristics, such as safe production, non-toxicity, high reactivity, chemical stability, electrochemical properties, biocompatibility, and low cost [22,23]. It is widely employed as a white pigment in plastics, paints, paper, and cosmetics [22], as well as a UV absorber, and antibacterial agent, in functional devices [24], semiconductors, and ceramics [25]. In addition, TiO_2 has been further used in glass, polyvinyl alcohol (PVA), and polycarbonate such as gamma-ray shielding [26], alkaline anion exchange membranes [27] and improved in environmental stress cracking [28], respectively. Furthermore, TiO_2 has been used as a high dielectric constant filler (approximately 100). In the last decade, the incorporation of TiO_2 into polymers to improve physical, thermal, mechanical, and dielectric properties has been explored. For example, Yang and Kofinas 2007 studied nano- TiO_2 -filled sulfonated styrene-*b*-(ethylene-*ran*-butylene)-*b*-styrene (S-SEBS) block copolymers by using vinyltrimethoxysilane as a crosslinker in order to decrease the dielectric loss from the free sulfonic acid groups [29]. Zhang et al. reported that rod-shaped TiO_2 nanoparticles act as effective fillers for improving the thermal stability and impact strength of rigid poly(vinyl chloride) (PVC) nanocomposites [30]. Qi et al. used surface-modified rutile-type titanium dioxide (CST) nanorods as a UV absorber in polypropylene (PP) [31], while Nasrin et al. investigated TiO_2 -filled isotactic polypropylene (iPP) composites with various TiO_2 contents. The dielectric constant decreased and the number of voids and holes on the composite surfaces increased with TiO_2 concentration, due to the incompatibility between TiO_2 and iPP matrix [32]. Madidi et al. demonstrated that the introduction of 5 wt.% nano- TiO_2 and 10 wt.% micro- TiO_2 improved the dielectric properties of silicone rubber/ TiO_2 composites. Additionally, an increased TiO_2 concentration increased the relative permittivity of the composite [33]. Commonly, TiO_2 has been utilized as an inexpensive inorganic pigment in rubber industries [34]. Nevertheless, the introduction of TiO_2 in the NBR for dielectric and mechanical properties via melt mixing is still largely unexplored. Some literature reports on polydopamine (PDA) coated nano- TiO_2 particles varying from 0 to 30 phr for improved TiO_2 dispersion in NBR by using peroxide cure system [35], but this showed an increase in tensile strength of the composites from 1.757 MPa for pure NBR to 2.287 for 30 phr TiO_2 -PDA/NBR. Peroxide-cured rubbers exhibit good aging resistance and low compression set at high temperatures, but the disadvantages include low scorch safety, tensile strength, tear strength, and worse dynamic and elastic properties compared to sulfur curing system [8,35]. This subsequently leads to the incorporation of TiO_2 microparticles within the NBR matrix using a sulfur curing system to improve the mechanical properties of composites.

In the present work, there is a great deal of interest in elastomeric composites with a high dielectric constant and robust mechanical properties. NBR composites were prepared by using micro- TiO_2 as reinforcing filler without any compatibilizer or coupling agent. The main purpose of this study was to investigate the influences of high TiO_2 loading varying from 0 to 110 phr on cure characteristics, and mechanical, and dielectric properties of the filled NBR composites.

2. Materials and Methods

2.1. Materials and Sample Preparation

Table 1 exhibits the materials, their suppliers, and formulation. Acrylonitrile butadiene rubber (NBR) with an acrylonitrile content of 33% was used in this research. Titanium dioxide (TiO_2) was analytical reagent grade with 99.5% purity, the particle size

is $21.69 \pm 10.33 \mu\text{m}$. All materials were used as received without any purification. Composites were blended in a 500 mL internal mixer at $60 \text{ }^\circ\text{C}$ with a rotor speed of 60 rpm. Mixing time and the sequence of adding ingredients were the same for all the composites, as listed in Table 1. Rubber compounds were sheeted out by using a two-roll mill and were kept at room temperature for 24 h before cure evaluation with a moving die rheometer (MDR) at $160 \text{ }^\circ\text{C}$ according to ASTM2240. The minimum torque (M_L) and maximum torque (M_H), torque difference ($M_H - M_L$), scorch time (t_{s1}), and cure time (t_{c90}) were acquired. Additionally, $150 \text{ mm} \times 160 \text{ mm} \times 2 \text{ mm}$ rubber composite sheets were obtained from compression molding at $160 \text{ }^\circ\text{C}$ for duration in accordance with their respective t_{c90} . Mooney viscosity ($M_L(1+4)$, $100 \text{ }^\circ\text{C}$) was determined at $100 \text{ }^\circ\text{C}$ with the large rotor for 4 min after preheating for 1 min according to ASTM D1646.

Table 1. Details of the materials and compounding formulations of TiO_2 -filled NBR composites.

Ingredient	Supplier	phr	Internal Mixer	Time (min)
NBR	Nantex public Co., Ltd. (Kaohsiung, Taiwan)	100	- Mastication of NBR	0
Sulphur	Vessel chemical public Co., Ltd. (Bangkok, Thailand)	1.5	- Addition of Sulphur	2
Zinc oxide	Bossoftical public Co., Ltd. (Songkla, Thailand)	5	- Addition of Zinc oxide	4
Stearic acid	Bossoftical public Co., Ltd. (Songkla, Thailand)	2	- Addition of stearic acid	6
MBTS	Vessel chemical public Co., Ltd. (Bangkok, Thailand)	1.5	- Addition of TiO_2	7
TiO_2	Labchem public Co., Ltd. (Surat Thani, Thailand)	0–110	- Addition of MBTS	10
			- Dumping	12

2.2. Characterization and Testing

A universal tensile test machine (Tinius Olsen, model 10ST, Salfords, England) was utilized to perform mechanical testing on rubber composites in accordance with ASTM D-412 at room temperature with a fixed extension speed of 500 mm/min at $23 \pm 2 \text{ }^\circ\text{C}$. The moduli at 100% and 300% elongation, as well as the tensile strength and elongation at break, are provided. The hardness of the NBR/ TiO_2 composites was tested using a Shore A durometer (Montech Rubber Testing Solutions, Hardness HT3000, Buchen, Germany) using 6 mm thick samples in accordance with ASTM D2240. Dynamic mechanical thermal analysis (DMTA 8000, PerkinElmer Inc., Waltham, MA, United States) was used to characterize the thermal analysis of NBR/ TiO_2 composites. The dynamic mechanical thermal experiment was carried out in tension mode at a heating rate of $3 \text{ }^\circ\text{C/min}$ and a strain of 0.1%. Temperature scanning and frequency scanning were carried out between $-50 \text{ }^\circ\text{C}$ and $50 \text{ }^\circ\text{C}$ as well as 0.1 Hz and 100 Hz, respectively. At $25 \text{ }^\circ\text{C}$, the dielectric constant of the vulcanizates was measured with an impedance analyzer (Agilent Technologies, Agilent 4285A, Santa Clara, CA, USA) across the frequency ranges of 10^2 – 10^5 Hz of AC at 1 V. The samples were placed between two parallel plates of the 5 mm diameter electrodes. SEM (FEI Quanta 400, Jeol Ltd., Tokyo, Japan) was utilized to detect TiO_2 dispersion in an NBR matrix. Cryogenic fracturing in liquid nitrogen was used to create a new cross-sectional surface for the samples. The fractured specimens were then sputtered with a thin layer of gold under a vacuum before being imaged.

3. Results and Discussion

3.1. Cure Characteristics of NBR/ TiO_2 Composites

Cure characteristics of the NBR composites with varied TiO_2 content are demonstrated and listed in Figure 1 and Table 2, respectively. The incorporation of TiO_2 caused a

shortened scorch time (t_{s1}) and cure time (t_{c90}). Increased TiO_2 content reduced t_{s1} and t_{c90} because TiO_2 metal oxide acts as a co-activator stimulating the crosslinking during sulfur curing. This is supported by the cure rate index (CRI) used to evaluate cure kinetics. The CRI increased with TiO_2 contents up to 30 phr and then remained constant. This supports the TiO_2 activating faster curing in the TiO_2 -filled NBR composites compared to the unfilled compound.

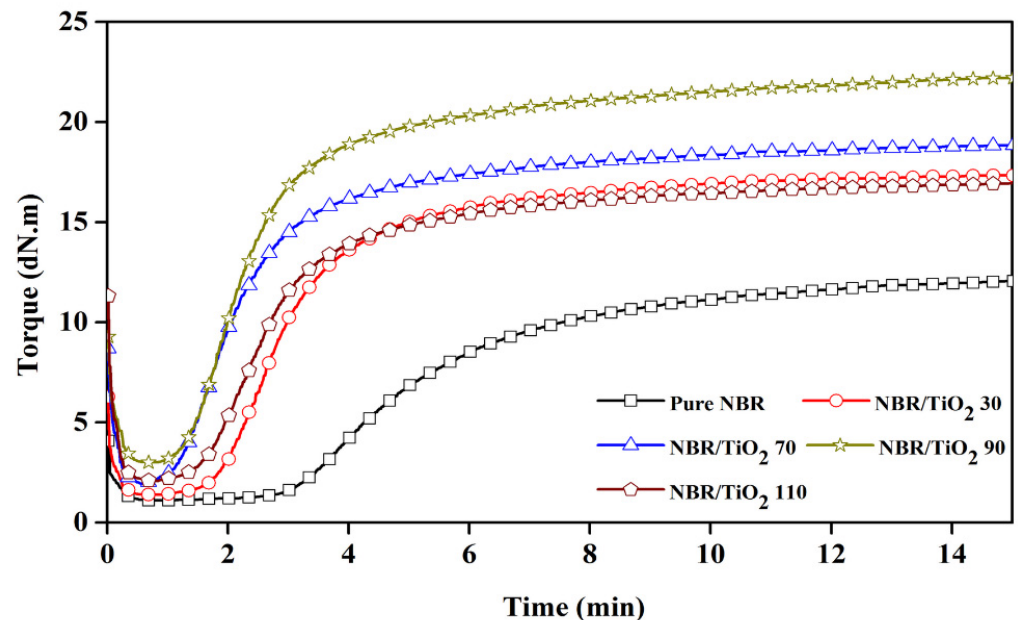


Figure 1. Cure curves of TiO_2 -filled NBR composites with various TiO_2 loadings.

Table 2. Cure characteristics and Mooney viscosity of TiO_2 -filled NBR composites with various TiO_2 loadings.

Sample	M_L (dN.m)	M_H (dN.m)	$M_H - M_L$ (dN.m)	t_{s1} (min)	t_{c90} (min)	CRI (min^{-1})	$M_L (1 + 4)$ 100 °C (MU)
Pure NBR	1.06	12.15	11.09	3.17	9.68	15.35	37.80
NBR/ TiO_2 30	1.36	16.54	15.18	2.03	6.00	25.21	46.10
NBR/ TiO_2 70	2.11	18.98	16.87	1.35	5.50	24.10	58.40
NBR/ TiO_2 90	3.00	22.20	19.20	1.47	5.90	22.56	64.30
NBR/ TiO_2 110	1.91	16.40	14.49	1.35	5.57	23.72	70.20

The viscosity of the compound and stiffness of the vulcanizes are indirectly reflected in the minimum torque (M_L) and the maximum torque (M_H), respectively. With increasing TiO_2 content, M_L displayed an increasing trend because TiO_2 particles obstructed molecular mobility with increased friction and high resistance to flow. However, M_L tended to decrease at 110 phr of TiO_2 content as a result of filler agglomeration. Figure 2 shows the correlation between the hardness of NBR filled with TiO_2 and viscosity. It is seen that TiO_2 -filled NBR composites exhibited much higher viscosities than virgin NBR due to the hydrodynamic effects of filler, filler–filler interactions, and filler–rubber interactions [36]. Moreover, the Mooney viscosities of TiO_2 -filled NBR composites increased from 37.8 to 70.2 MU with TiO_2 loading, since an increased number of solid particles in the soft matrix caused more movement restrictions [37].

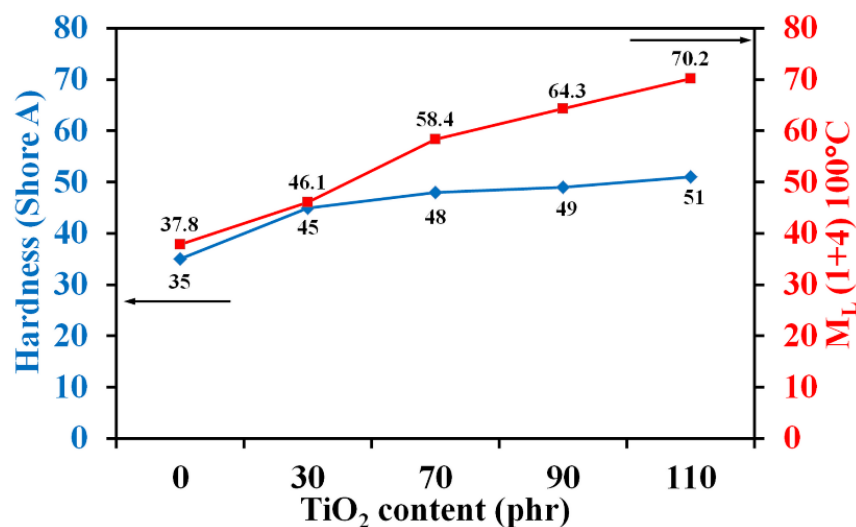
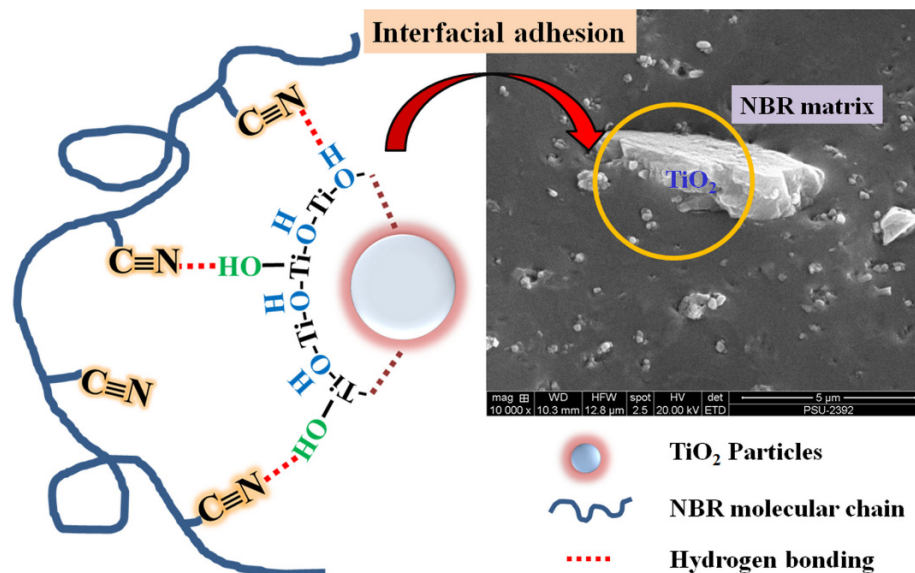


Figure 2. Mooney viscosity and hardness of TiO₂-filled NBR composites with various TiO₂ loadings.

The torque difference ($M_H - M_L$) indirectly reflects the crosslink density in rubber vulcanizates. $M_H - M_L$ increased with the addition of TiO₂ indicating a higher crosslink density caused by TiO₂ due to strong filler–rubber interactions: the physical interactions between polar $-C\equiv N$ groups in NBR and $-OH$ groups on TiO₂ surfaces. These surface hydroxyl groups, both of terminal OH and bridge OH, were generated by the reaction of surface oxide with moisture in the air [38,39]. The proposed physical interaction in TiO₂-filled NBR composites is shown in Scheme 1.



Scheme 1. Schematic diagram illustrating physical bonding and interfacial adhesion in TiO₂-filled NBR composites.

3.2. Mechanical Properties

Figure 3 displays the stress–strain curves of the NBR composites. Pure NBR exhibited the lowest stress–strain curve with elongation at break $\sim 550\%$, and without self-reinforcing behavior due to the irregular random copolymer structure, leading to insufficient mechanical properties [9]. It was found that the stress steadily increased with applied strain and then escalated sharply for TiO₂-filled NBR composites. The abrupt increase in stress was observed at a high strain ($>500\%$ strain), especially with 90 phr TiO₂ content, as opposed to the unfilled NBR composite that did not show strain-induced crystallization. The strain

at the onset of the stress upturn corresponded to the onset of crystallization [40]. In the presence of TiO_2 , stronger chain alignment in the strain direction was caused by the additional crosslinks created by filler–rubber interactions [41], as seen in Scheme 2. This corroborates that the NBR molecular chain orientation was assisted by TiO_2 particles, to perform interfacial crystallization during stretching. Moreover, TiO_2 -filled NBR composites showed an increased slope of the stress–strain curve compared to pure NBR, indicating stiffening. This matches the responses in M_H and hardness discussed earlier.

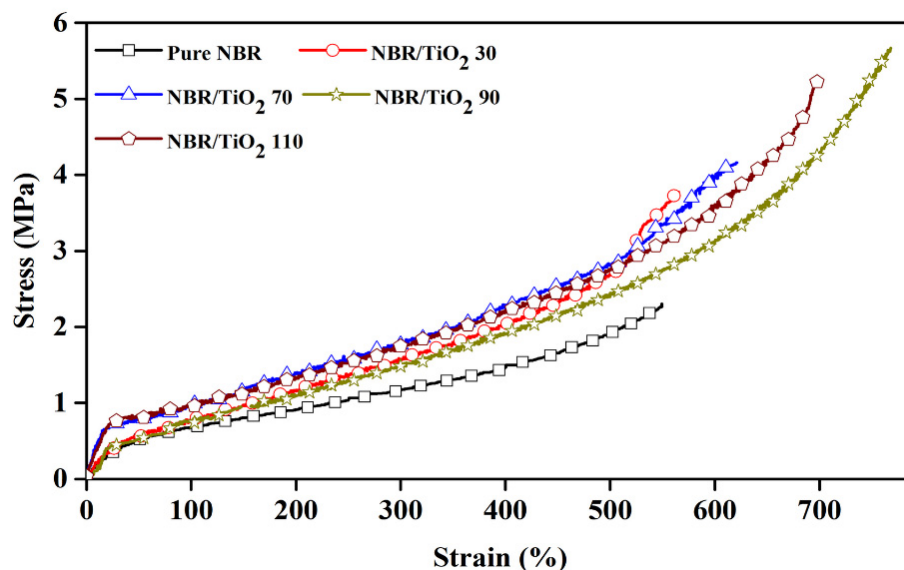
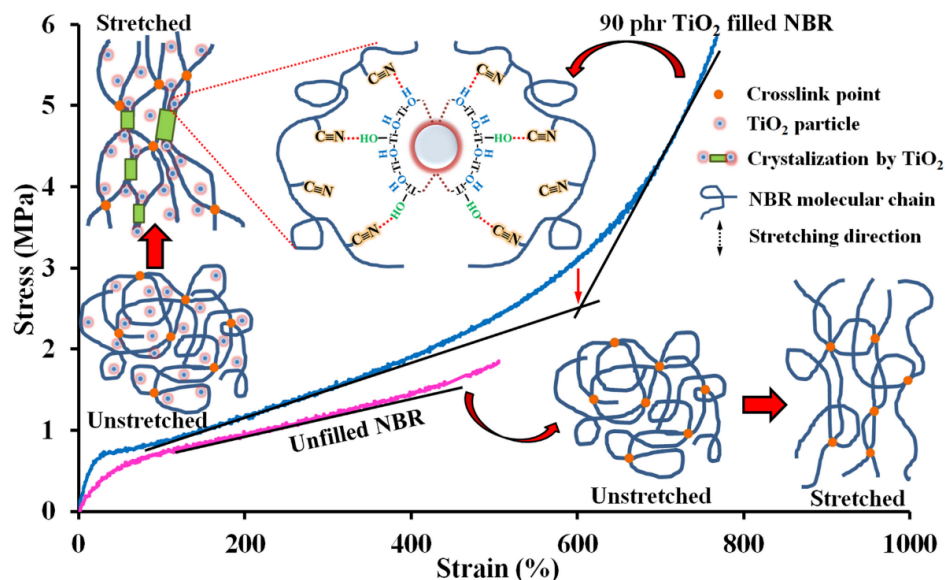


Figure 3. Stress–strain behavior of TiO_2 -filled NBR composites with various TiO_2 loadings.



Scheme 2. Schematic illustration of the proposed reinforcing mechanism and strain-induced crystallization in TiO_2 -filled NBR composites.

Table 3 lists the mechanical properties of the various NBR composites. Most mechanical properties, namely tensile strength, elongation at break, moduli at 100% and 300% elongations, and hardness, increased with TiO_2 loading indicating that this acted as a reinforcing filler in the NBR matrix. Tensile strength and elongation at break improved with increasing TiO_2 content from 0 phr to a maximum at 90 phr. The 90 phr TiO_2 content showed a 144.8% increase in tensile strength and a 40.1% increase in elongation at break. This was primarily attributed to the good filler–rubber interactions leading to a good filler

dispersion in the NBR matrix and efficient stress transfer from matrix to filler [42]. A good ability in a composite to transfer applied stress relies on strong filler–matrix interactions. Secondly, the compatibility of –OH functional groups in TiO₂ and –C≡N can create strong filler–matrix interfacial adhesion (Scheme 1). Consequently, the filler–filler bonds and filler–rubber bonds in TiO₂-filled NBR composites contributed to the total crosslinking [43]. On further increasing TiO₂ content up to 110 phr, the tensile strength and elongation at break slightly decreased, probably due to agglomeration of TiO₂ in the NBR matrix and thereby degraded filler–rubber interactions [44], while the matrix phase continuity was also impeded. Stress transfer was obstructed and weaker composites with lower tensile strength, lesser flexibility, and higher stiffness were obtained [45].

Table 3. Mechanical properties of TiO₂-filled NBR composites with various TiO₂ loadings.

Sample	σ_b (MPa)	ϵ_b (%)	M100 (MPa)	M300 (MPa)	Reinforcing Index	Hardness (Shore A)
Pure NBR	2.82 ± 0.11	550 ± 15	0.71 ± 0.01	1.20 ± 0.04	1.69	35
NBR/TiO ₂ 30	3.77 ± 0.16	565 ± 15	1.01 ± 0.07	2.08 ± 0.05	2.06	45
NBR/TiO ₂ 70	4.16 ± 0.18	621 ± 14	1.21 ± 0.02	2.59 ± 0.05	2.14	48
NBR/TiO ₂ 90	5.68 ± 0.13	768 ± 11	1.45 ± 0.01	2.79 ± 0.04	1.92	49
NBR/TiO ₂ 110	5.24 ± 0.18	699 ± 19	1.50 ± 0.03	2.87 ± 0.03	1.91	51

Moduli at 100% and 300% elongations are indirectly correlated to stiffness and rigidity. Table 3 shows that the moduli at 100% and 300% elongations were higher for TiO₂-filled composites than for unfilled vulcanizate. The moduli at 100% and 300% elongations were increased by 111% and 139%, respectively, for NBR composites with 110 phr TiO₂ content. This indicates that the stiffness of the composites had increased due to crosslinking, in agreement with M_H and $M_H - M_L$ results previously discussed with the cure characteristics. Considering the reinforcing index, the ratio of the modulus at 300% elongation to modulus at 100% elongation (M_{300}/M_{100}) [36], was higher for TiO₂-filled NBR composites than for pure NBR vulcanizate. This was probably due to good interactions between NBR rubber and TiO₂ filler. This is confirming that TiO₂ acted as a reinforcing filler in NBR rubber. The 70 phr TiO₂-filled composites exhibited the highest reinforcement index. On further increasing TiO₂ content, the reinforcement index tended to decrease due to filler agglomeration.

The resistance to surface penetration by a material is evaluated by its hardness. It was found that the hardness of NBR composites is affected by TiO₂ content as seen in Table 3. The NBR composite reinforced with 110 phr TiO₂ loading exhibited an increase of approximately 46% from the hardness of the pure NBR vulcanizate. This is explained by the increased crosslink density in NBR composites, related to the higher torque difference seen earlier, as well as the rigid inorganic TiO₂ particles being noticeably stiffer than the rubber matrix [46]. As more TiO₂ particles were introduced into the NBR matrix, the elasticity diminished [47]. Chokanandsombat and Sirisinha explained an increase in hardness with a dynamic effect in which the rubber matrix was diluted by rigid metal oxide fillers [48]. Moreover, an increase in the TiO₂ loading of the NBR matrix reduced the free volume because of the filling of the space by complex formations of Ti³⁺ and O[−] ions [27], leading to increased resistance to indentation for the composite.

3.3. Morphology Characterization

SEM was used to determine the compatibility and dispersion of filler in the rubber matrix which affected the properties of the filled composites. Figure 4 exhibits SEM micrographs taken from fracture surfaces of NBR composites. Smooth surfaces are seen in Figure 4a due to the lack of an inorganic filler in the NBR matrix. SEM images support the prior tensile properties. This shows that incorporating TiO₂ in the NBR matrix induced rougher fracture surfaces so more energy was needed to break the sample. The strong hydrogen bonds between TiO₂ particles and the NBR matrix can prevent the formation

of defects that initiate or propagate fractures. This matches the improved mechanical properties TiO₂-filled composites compared to pure NBR vulcanizate. Good dispersion and compatibility (Scheme 2) between TiO₂ and NBR played major roles in improved stress transfer between the NBR rubber matrix and TiO₂ filler. However, some cavities (yellow circle) and TiO₂ aggregates (red circle) in the NBR matrix were evidenced when TiO₂ loading exceeded 90 phr (Figure 4c) so less energy was needed for failure.

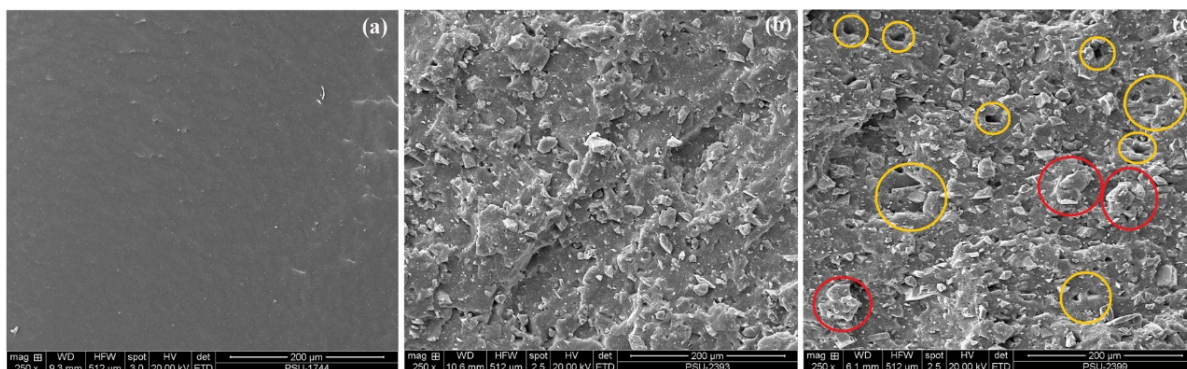


Figure 4. SEM images of fracture surfaces on TiO₂-filled NBR composites with (a) 0 phr TiO₂ (or pure NBR), (b) 70 phr TiO₂, and (c) 110 phr TiO₂.

3.4. Dynamic Mechanical Analysis

Dynamic mechanical properties inform about storage modulus, loss modulus, and loss tangent ($\tan \delta$). The storage modulus relates to the stiffness, while the loss modulus is associated with viscous response. $\tan \delta$ is the ratio of loss modulus to storage modulus, relating to the molecular mobility and phase transition [49].

Figure 5a,b show the typical variation with temperature in storage modulus and $\tan \delta$, respectively, at the frequencies 0.1, 1, 10 and 100 Hz for pure NBR. Since rubber is a viscoelastic material, its properties display time dependence where a high frequency translates into a short time. It was found that the storage modulus increased and shifted to higher temperature with increasing frequency, as seen in Figure 5a. This was because the rubber chains have little time to transition during high-frequency cyclic deformation, resulting in the material behaving more like an elastic solid with a larger storage modulus [50]. In addition, at a higher frequency, a peak or hump (red circle in Figure 5a) was observed in the storage modulus because molecular rearrangement eased the stress that had been trapped at temperatures below the glass transition temperature (T_g) [51]. The dynamic mechanical thermal analysis represents an alternative method for measuring the glass transition temperature, which is the identified location of the $\tan \delta$ peak. At T_g , the expanding volume of the material with increasing temperature becomes sufficient to allow chain flow. It is clear that T_g increased with frequency from -20.3 °C to -4.1 °C, as shown in Figure 5b, while the intensity of $\tan \delta$ peak tended to increase due to the rubber composite behaving more like an elastic solid at a higher frequency of deformation [50].

In addition, dynamic mechanical properties are used to assess the interactions between the inorganic TiO₂-filler particles and the NBR matrix. Temperature dependence of the storage modulus (E') and of $\tan \delta$ are shown in Figure 5c,d, respectively. Figure 5c demonstrates that typical behavior of all storage modulus curves for vulcanized rubber, with three distinct states: the glassy high modulus state at very low temperature where molecule movements are tightly compressed; the transition state where the storage modulus sharply declines related to the coordinated chain segments in the amorphous phase simultaneously moving; and the rubbery plateau with modulus correlated to crosslink density or chain length between entanglements [51,52]. Increasing TiO₂ content in the NBR matrix increased E' in both the glassy and the rubbery regions. This was attributed to the stiffening effects of TiO₂ rigid filler along with its interactions with the NBR matrix. In Figure 5d, the peak position of the $\tan \delta$ is plotted, identifying T_g affected by the mobility of molecular

segments. Relatively low $\tan \delta$ is observed both below and above T_g . This is because the molecular chains are immobilized and restricted in the glassy state, while the molecular chains can move more freely in the rubbery state. The slight shift in the T_g to higher temperatures with TiO_2 loading was due to the good filler–rubber interactions limiting chain mobility, resulting in higher energy required for mobility. In addition, pure NBR has the highest $\tan \delta$ at ~ 1.62 due to its flexible elastomer nature. $\tan \delta$ tends to decrease with TiO_2 loading because of filler–rubber interactions via hydrogen bonds acting as physical crosslinks, obstructing chain mobility in TiO_2 -filled composites, and causing a less effective response to cyclic loading. The shift of T_g toward higher temperatures and decrease in $\tan \delta$ support good compatibility between TiO_2 filler and NBR rubber matrix.

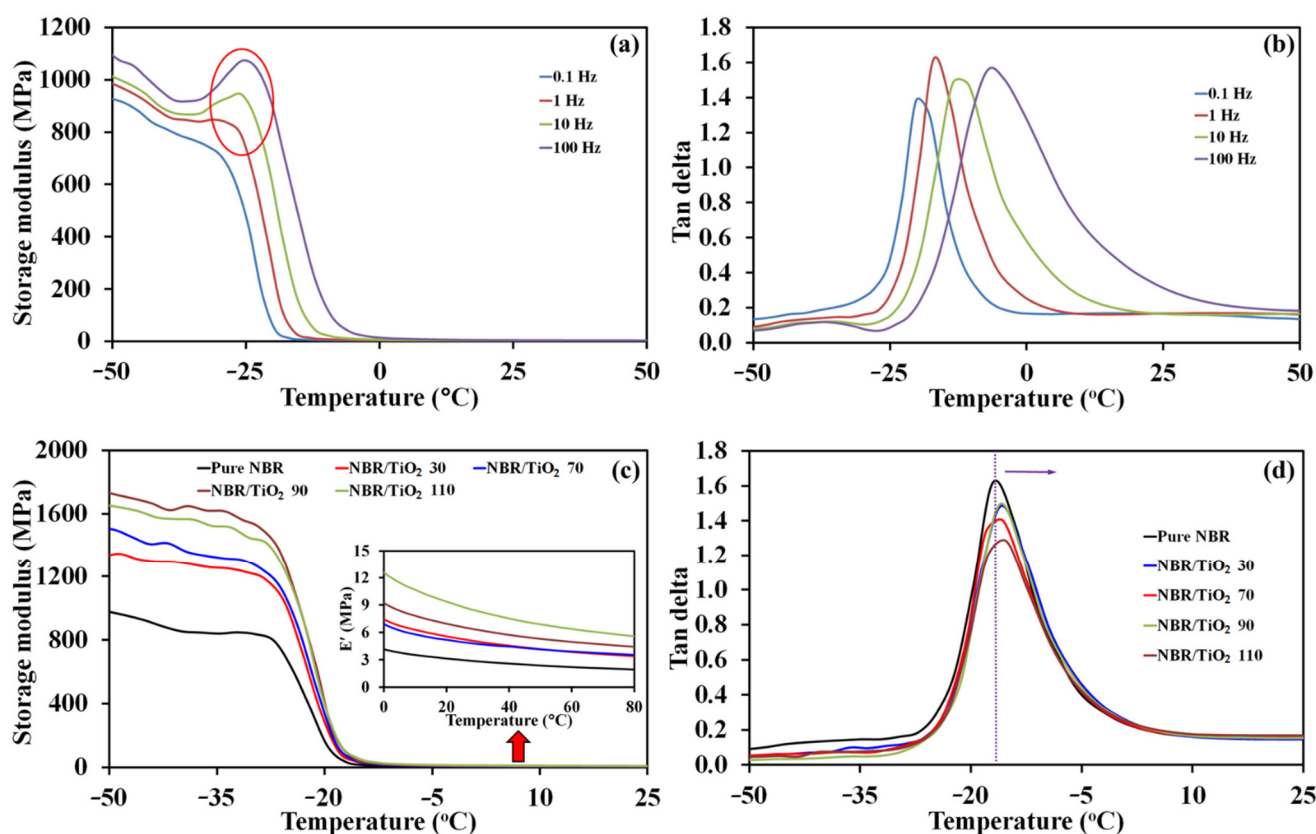


Figure 5. (a) Storage modulus, and (b) $\tan \delta$ as functions of temperature for pure NBR at several frequencies; (c) storage modulus, and (d) $\tan \delta$ as functions of temperature for TiO_2 -filled NBR composites with various TiO_2 loadings at 1 Hz.

3.5. Dielectric Properties of NBR/ TiO_2 Composites

Figure 6 displays the dielectric constant versus frequency for different TiO_2 loadings in NBR composites. There is a noticeable reduction in dielectric constant with frequency from 10^2 to 10^5 Hz in all cases because the electrical polarization is harder to follow at a higher frequency [53]. The maximum (~ 18.83) for pure NBR was observed at 10^2 Hz because of strong contributions from interfacial and dipolar polarization in the low-frequency range [54]. The high dielectric constant of pure NBR was due to the orientation polarization of the $-\text{C}\equiv\text{N}$ dipoles. On increasing the frequency to 10^5 Hz, the dielectric constant decreased. This might be because the dipoles are incapable of reorienting rapidly enough to follow the applied frequency. With the introduction of TiO_2 , the dielectric constant of TiO_2 -filled composites increased with increasing TiO_2 content because TiO_2 has a higher dielectric constant than pure NBR. The 110 phr TiO_2 -filled composites showed the highest dielectric constant of 20.28 at a frequency of 10^2 Hz. Furthermore, the increased dielectric constant was partly attributed to better dipole orientation polarization due to the segment

arrangement of rubber chains [55]. After the incorporation of TiO_2 filler, the composites had more interfaces enabling interfacial polarization [56].

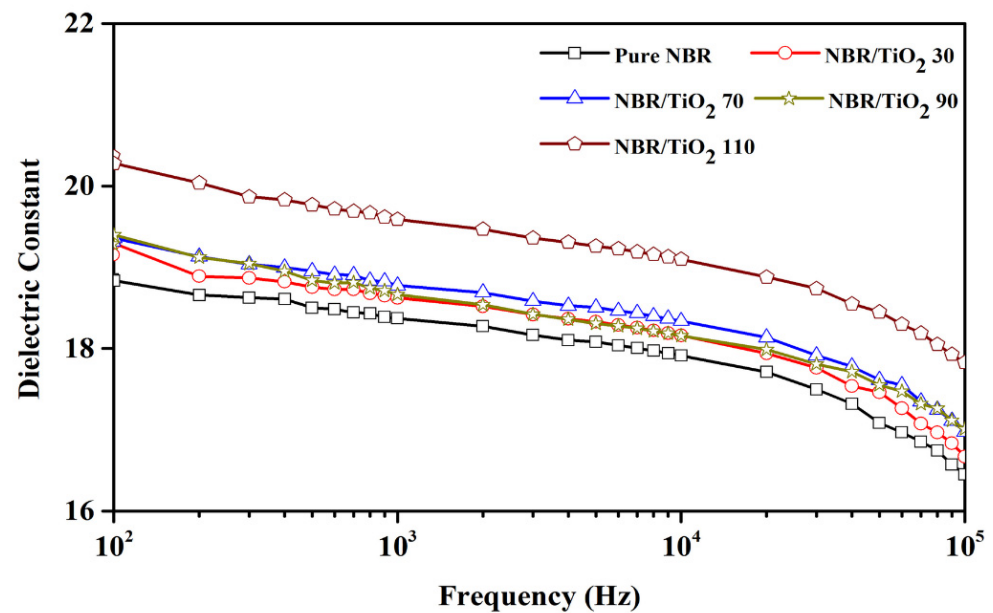


Figure 6. Dielectric constant of TiO_2 -filled NBR composites with various TiO_2 loadings.

4. Conclusions

TiO_2 was incorporated as filler into NBR with loadings up to 110 phr. It has good compatibility and disperses efficiently in the NBR matrix due to the strong filler-rubber interactions via hydrogen bonds between hydroxyl on the TiO_2 surface and acrylonitrile-functional groups, resulting in an increased cure rate index and crosslink density in TiO_2 -filled compounds. Accordingly, improved tensile strength, elongation at break, moduli at 100% and 300% elongations, and hardness were obtained. The 90 phr TiO_2 content resulted in a 144.8% increase in tensile strength and a 40.1% increase in elongation at break. This was primarily due to good filler-rubber interactions, which resulted in good filler dispersion in the NBR matrix and efficient stress transfer from matrix to filler. The addition of TiO_2 resulted in an increase in storage modulus, a slight shift in T_g upward, and less mechanical damping. The presence of TiO_2 in the composites increased the dielectric constant of filled NBR. The 110 phr TiO_2 -filled composites had the highest dielectric constant of 20.28 at 10^2 Hz. High dielectric constant and strong mechanical properties are two benefits of the TiO_2 -filled composites that were obtained. As a result, it could be implemented in dielectric elastomer actuators application.

Author Contributions: Methodology, P.L.; writing—original draft preparation, W.C.; writing—review and editing, N.C. All authors have read and agreed to the published version of the manuscript.

Funding: This research was funded by the government budget of Prince of Songkla University and Natural Rubber Innovation Research Institute (NR-IRI), grant number SIT610284S.

Institutional Review Board Statement: Not applicable.

Data Availability Statement: Data presented in this study are available on request from the corresponding author.

Acknowledgments: We are grateful to Seppo Karrila for his assistance with manuscript preparation.

Conflicts of Interest: The authors declare no conflict of interest.

References

1. Yang, D.; Huang, S.; Wu, Y.; Ruan, M.; Li, S.; Shang, Y.; Cui, X.; Wang, Y.; Guo, W. Enhanced Actuated Strain of Titanium Dioxide/Nitrile-Butadiene Rubber Composite by the Biomimetic Method. *RSC Adv.* **2015**, *5*, 65385–65394. [[CrossRef](#)]
2. Franke, M.; Ehrenhofer, A.; Lahiri, S.; Henke, E.-F.M.; Wallmersperger, T.; Richter, A. Dielectric Elastomer Actuator Driven Soft Robotic Structures With Bioinspired Skeletal and Muscular Reinforcement. *Front. Robot. AI* **2020**, *7*, 510757. [[CrossRef](#)] [[PubMed](#)]
3. Madsen, F.B.; Yu, L.; Daugaard, A.E.; Hvilsted, S.; Skov, A.L. Silicone Elastomers with High Dielectric Permittivity and High Dielectric Breakdown Strength Based on Dipolar Copolymers. *Polymer* **2014**, *55*, 6212–6219. [[CrossRef](#)]
4. Skov, A.L.; Pei, Q.; Opris, D.; Spontak, R.J.; Gallone, G.; Shea, H.; Benslimane, M.Y. Dielectric Elastomers (DEs) as EAPs: Materials. In *Electromechanically Active Polymers*; Carpi, F., Ed.; Springer International Publishing: Cham, Germany, 2016; pp. 687–714. [[CrossRef](#)]
5. Kanny, K.; Mohan, T.P. Rubber Nanocomposites with Nanoclay as the Filler. In *Progress in Rubber Nanocomposites*; Elsevier: Amsterdam, The Netherlands, 2017; pp. 153–177. [[CrossRef](#)]
6. Li, T.; Shi, Z.; He, X.; Jiang, P.; Lu, X.; Zhang, R.; Wang, X. Aging-Resistant Functionalized LDH-SAS/Nitrile-Butadiene Rubber Composites: Preparation and Study of Aging Kinetics/Anti-Aging Mechanism. *Materials* **2018**, *11*, 836. [[CrossRef](#)]
7. Valentini, L.; Bittolo Bon, S.; Hernández, M.; Lopez-Manchado, M.A.; Pugno, N.M. Nitrile Butadiene Rubber Composites Reinforced with Reduced Graphene Oxide and Carbon Nanotubes Show Superior Mechanical, Electrical and Icephobic Properties. *Compos. Sci. Technol.* **2018**, *166*, 109–114. [[CrossRef](#)]
8. El-Nemr, K.F. Effect of Different Curing Systems on the Mechanical and Physico-Chemical Properties of Acrylonitrile Butadiene Rubber Vulcanizates. *Mater. Des.* **2011**, *32*, 3361–3369. [[CrossRef](#)]
9. Kapgate, B.P.; Das, C.; Basu, D.; Das, A.; Heinrich, G. Rubber Composites Based on Silane-Treated Stöber Silica and Nitrile Rubber: Interaction of Treated Silica with Rubber Matrix. *J. Elastomers Plast.* **2015**, *47*, 248–261. [[CrossRef](#)]
10. de Sousa, F.D.B.; Mantovani, G.L.; Scuracchio, C.H. Mechanical Properties and Morphology of NBR with Different Clays. *Polym. Test.* **2011**, *30*, 819–825. [[CrossRef](#)]
11. Balachandran, M.; Devanathan, S.; Muraleekrishnan, R.; Bhagawan, S.S. Optimizing Properties of Nanoclay–Nitrile Rubber (NBR) Composites Using Face Centred Central Composite Design. *Mater. Des.* **2012**, *35*, 854–862. [[CrossRef](#)]
12. Sadek, E.M.; El-Nashar, D.E.; Ahmed, S.M. Influence of Modifying Agents of Organoclay on the Properties of Nanocomposites Based on Acrylonitrile Butadiene Rubber. *Egypt. J. Pet.* **2018**, *27*, 1177–1185. [[CrossRef](#)]
13. Cho, J.-H. Effect of Carbon Black Activation on Physicomechanical Properties of Butadiene-Nitrile Rubber. *Bull. Korean Chem. Soc.* **2014**, *35*, 2891–2894. [[CrossRef](#)]
14. Al-maamori, M.H.; AL-Zubaidi, A.A.M.; Subeh, A.A. Effect of Carbon Black on Mechanical and Physical Properties of Acrylonitrile Butadiene Rubber (NBR) Composite. *Acad. Res. Int.* **2015**, *6*, 28–37.
15. Shankar, U.; Bhandari, S.; Khastgir, D. Carbon Black-Filled Nitrile Rubber Composite as a Flexible Electrode for Electrochemical Synthesis of Supercapacitive Polyaniline. *Polym. Compos.* **2019**, *40*, E1537–E1547. [[CrossRef](#)]
16. Boonbumrung, A.; Sae-oui, P.; Sirisinha, C. Reinforcement of Multiwalled Carbon Nanotube in Nitrile Rubber: In Comparison with Carbon Black, Conductive Carbon Black, and Precipitated Silica. *J. Nanomater.* **2016**, *2016*, 6391572. [[CrossRef](#)]
17. Tsongas, K.; Tzetzis, D.; Mansour, G. Mechanical and Vibration Isolation Behaviour of Acrylonitrile-Butadiene Rubber/Multi-Walled Carbon Nanotube Composite Machine Mounts. *Plast. Rubber Compos.* **2017**, *46*, 458–468. [[CrossRef](#)]
18. Keinänen, P.; Das, A.; Vuorinen, J. Further Enhancement of Mechanical Properties of Conducting Rubber Composites Based on Multiwalled Carbon Nanotubes and Nitrile Rubber by Solvent Treatment. *Materials* **2018**, *11*, 1806. [[CrossRef](#)]
19. Suzuki, N.; Ito, M.; Ono, S. Effects of Rubber/Filler Interactions on the Structural Development and Mechanical Properties of NBR/Silica Composites. *J. Appl. Polym. Sci.* **2005**, *95*, 74–81. [[CrossRef](#)]
20. Thomas, O.; Namboothiri, V.N.N.; Joseph, R. Feasibility of Silica Loaded NBR as Lining Material for Impactive Gripper. *Procedia Technol.* **2016**, *25*, 900–907. [[CrossRef](#)]
21. Eyssa, H.M.; Abulyazied, D.E.; Abdulrahman, M.; Youssef, H.A. Mechanical and Physical Properties of Nanosilica/Nitrile Butadiene Rubber Composites Cured by Gamma Irradiation. *Egypt. J. Pet.* **2018**, *27*, 383–392. [[CrossRef](#)]
22. Alghamdi, M.N. Titanium Dioxide Reinforced Polypropylene Composites: Preparation and Characterization. *Int. J. Eng. Res. Technol.* **2016**, *5*, 633–637.
23. Anaya-Esparza, L.M.; Villagrán-de la Mora, Z.; Ruvalcaba-Gómez, J.M.; Romero-Toledo, R.; Sandoval-Contreras, T.; Aguilera-Aguirre, S.; Montalvo-González, E.; Pérez-Larios, A. Use of Titanium Dioxide (TiO₂) Nanoparticles as Reinforcement Agent of Polysaccharide-Based Materials. *Processes* **2020**, *8*, 1395. [[CrossRef](#)]
24. Awang, M.; Mohd, W.R.W. Comparative Studies of Titanium Dioxide and Zinc Oxide as a Potential Filler in Polypropylene Reinforced Rice Husk Composite. *IOP Conf. Ser. Mater. Sci. Eng.* **2018**, *342*, 012046. [[CrossRef](#)]
25. Siwińska-Stefańska, K.; Ciesielczyk, F.; Nowacka, M.; Jesionowski, T. Influence of Selected Alkoxysilanes on Dispersive Properties and Surface Chemistry of Titanium Dioxide and TiO₂-SiO₂ Composite Material. *J. Nanomater.* **2012**, *2012*, 316173. [[CrossRef](#)]
26. Alharbi, T.; Mohamed, H.F.M.; Saddeek, Y.B.; El-Haseib, A.Y.; Shaaban, K.S. Study of the TiO₂ Effect on the Heavy Metals Oxides Borosilicate Glasses Structure Using Gamma-Ray Spectroscopy and Positron Annihilation Technique. *Radiat. Phys. Chem.* **2019**, *164*, 108345. [[CrossRef](#)]
27. Abdel-Hady, E.E.; Mohamed, H.F.M.; Abdel-Hamed, M.O.; Gomaa, M.M. Physical and Electrochemical Properties of PVA/TiO₂ Nanocomposite Membrane. *Adv. Polym. Technol.* **2018**, *37*, 3842–3853. [[CrossRef](#)]

28. Khalid, Y.; Achour, A.; Akram, M.A.; Islam, M. Polycarbonate/Titania Composites Incorporating TiO₂ with Different Nanoscale Morphologies for Enhanced Environmental Stress Cracking Resistance in Dioctyl Phthalate. *Polymers* **2022**, *14*, 3693. [[CrossRef](#)]
29. Yang, T.-I.; Kofinas, P. Dielectric Properties of Polymer Nanoparticle Composites. *Polymer* **2007**, *48*, 791–798. [[CrossRef](#)]
30. Zhang, Y.; Song, Y.; Zheng, Q. Mechanical and Thermal Properties of Nanosized Titanium Dioxide Filled Rigid Poly(Vinyl Chloride). *Chin. J. Polym. Sci.* **2013**, *31*, 325–332. [[CrossRef](#)]
31. Qi, L.; Ding, Y.; Dong, Q.; Wen, B.; Liu, P.; Wang, F.; Zhang, S.; Yang, M. UV Photodegradation of Polypropylene Thick Bars Containing Rutile-Type TiO₂ Nanorods. *Chin. J. Polym. Sci.* **2014**, *32*, 834–843. [[CrossRef](#)]
32. Nasrin, R.; Seema, S.; Gafur, M.A.; Bhuiyan, A.H. Study of Dielectric Behavior of Titanium Dioxide-Filled Polypropylene Composites. *Am. J. Mater. Synth. Process.* **2018**, *3*, 56–61. [[CrossRef](#)]
33. Madidi, F.; Momen, G.; Farzaneh, M. Dielectric Properties of TiO₂/Silicone Rubber Micro- and Nanocomposites. *Adv. Mater. Sci. Eng.* **2018**, *2018*, 4682076. [[CrossRef](#)]
34. Seentrakoon, B.; Junhasavasdikul, B.; Chavasiri, W. Enhanced UV-Protection and Antibacterial Properties of Natural Rubber/Rutile-TiO₂ Nanocomposites. *Polym. Degrad. Stab.* **2013**, *98*, 566–578. [[CrossRef](#)]
35. Kruželák, J.; Kvasničáková, A.; Medlenová, E.; Dosoudil, R.; Hudec, I. Application of Peroxide Curing Systems in Cross-Linking of Rubber Magnets Based on NBR and Barium Ferrite. *Adv. Mater. Sci. Eng.* **2019**, *2019*, 1640548. [[CrossRef](#)]
36. Kaewsakul, W.; Sahakaro, K.; Dierkes, W.K.; Noordermeer, J.W.M. Optimization of Mixing Conditions for Silica-Reinforced Natural Rubber Tire Tread Compounds. *Rubber Chem. Technol.* **2012**, *85*, 277–294. [[CrossRef](#)]
37. Phuihangpa, N.; Ponloa, W.; Phongphanphane, S.; Smitthipong, W. Performance of Nano- and Microcalcium Carbonate in Uncrosslinked Natural Rubber Composites: New Results of Structure–Properties Relationship. *Polymers* **2020**, *12*, 2002. [[CrossRef](#)]
38. Hanawa, T. A Comprehensive Review of Techniques for Biofunctionalization of Titanium. *J. Periodontal. Implant Sci.* **2011**, *41*, 263. [[CrossRef](#)] [[PubMed](#)]
39. Pivkina, A.N.; Muravyev, N.V.; Monogarov, K.A.; Fomenkov, I.V.; Schoonman, J. Catalysis of HMX Decomposition and Combustion. In *Energetic Nanomaterials*; Elsevier: Amsterdam, The Netherlands, 2016; pp. 193–230. [[CrossRef](#)]
40. Chenal, J.-M.; Gauthier, C.; Chazeau, L.; Guy, L.; Bomal, Y. Parameters Governing Strain Induced Crystallization in Filled Natural Rubber. *Polymer* **2007**, *48*, 6893–6901. [[CrossRef](#)]
41. Bokobza, L. Mechanical and Electrical Properties of Elastomer Nanocomposites Based on Different Carbon Nanomaterials. *C* **2017**, *3*, 10. [[CrossRef](#)]
42. El-Nashar, D.E.; Mansour, S.H.; Girgis, E. Nickel and Iron Nano-Particles in Natural Rubber Composites. *J. Mater. Sci.* **2006**, *41*, 5359–5364. [[CrossRef](#)]
43. Hang, L.T.; Viet, D.Q.; Linh, N.P.D.; Doan, V.A.; Dang, H.-L.T.; Dao, V.-D.; Tuan, P.A. Utilization of Leather Waste Fibers in Polymer Matrix Composites Based on Acrylonitrile-Butadiene Rubber. *Polymers* **2020**, *13*, 117. [[CrossRef](#)] [[PubMed](#)]
44. Nor, N.A.M.; Othman, N. Effect of Filler Loading on Curing Characteristic and Tensile Properties of Polygorskite Natural Rubber Nanocomposites. *Procedia Chem.* **2016**, *19*, 351–358. [[CrossRef](#)]
45. Mente, P.; Motaung, T.E.; Hlangothi, S.P. Natural Rubber and Reclaimed Rubber Composites—A Systematic Review. *Polym. Sci.* **2016**, *2*, 1–7. [[CrossRef](#)]
46. Kundie, F.; Azhari, C.H.; Muchtar, A.; Ahmad, Z.A. Effects of Filler Size on the Mechanical Properties of Polymer-Filled Dental Composites: A Review of Recent Developments. *JPS* **2018**, *29*, 141–165. [[CrossRef](#)]
47. Hayemasae, N.; Rathnayake, W.G.I.U.; Ismail, H. Nano-Sized TiO₂-Reinforced Natural Rubber Composites Prepared by Latex Compounding Method. *J. Vinyl. Addit. Technol.* **2017**, *23*, 200–209. [[CrossRef](#)]
48. Chokanandsombat, Y.; Sirisinha, C. MgO and ZnO as Reinforcing Fillers in Cured Polychloroprene Rubber. *J. Appl. Polym. Sci.* **2013**, *128*, 2533–2540. [[CrossRef](#)]
49. Hamdan, S.; Hasihim, D.M.A.; Yusop, M. Dynamic Mechanical Thermal Analysis (DMTA) of Thermoplastic Natural Rubber (TPNR) Barium Ferrite (BaFe₁₂O₁₉) Composites. *AJSTD* **2017**, *21*, 69. [[CrossRef](#)]
50. Rico, A.; Outón, P.R.; Salazar, A.; Benavente, R.; Rodríguez, J. Strain Rate and Loading Modes in DMTA Experiments on Ethylene/Propylene Block Copolymers. *Mech. Time-Depend. Mater.* **2014**, *18*, 407–422. [[CrossRef](#)]
51. Menard, K.P.; Menard, N.R. Dynamic Mechanical Analysis in the Analysis of Polymers and Rubbers. In *Encyclopedia of Polymer Science and Technology*; John Wiley & Sons, Inc., Ed.; Wiley: Hoboken, NJ, USA, 2015; pp. 1–33. [[CrossRef](#)]
52. Komalan, C.; George, K.E.; Kumar, P.A.S.; Varughese, K.T.; Thomas, S. Dynamic Mechanical Analysis of Binary and Ternary Polymer Blends Based on Nylon Copolymer/EPDM Rubber and EPM Grafted Maleic Anhydride Compatibilizer. *Express Polym. Lett.* **2007**, *1*, 641–653. [[CrossRef](#)]
53. Badr, A.M.; Elshaiikh, H.A.; Ashraf, I.M. Impacts of Temperature and Frequency on the Dielectric Properties for Insight into the Nature of the Charge Transports in the Ti2S Layered Single Crystals. *JMP* **2011**, *2*, 12–25. [[CrossRef](#)]
54. Nayak, S.; Rahaman, M.; Pandey, A.K.; Setua, D.K.; Chaki, T.K.; Khastgir, D. Development of Poly(Dimethylsiloxane)-Titania Nanocomposites with Controlled Dielectric Properties: Effect of Heat Treatment of Titania on Electrical Properties. *J. Appl. Polym. Sci.* **2013**, *127*, 784–796. [[CrossRef](#)]
55. Ward, A.; El-Sabbagh, S.H.; El-Ghaffar, M.A.A. Studies on the Dielectric and Physical Properties of Phosphate Pigment/Rubber Composites. *KGK Rubberpoint* **2013**, *6*, 29–40.
56. Tu, L.; Xiao, Q.; Wei, R.; Liu, X. Fabrication and Enhanced Thermal Conductivity of Boron Nitride and Polyarylene Ether Nitrile Hybrids. *Polymers* **2019**, *11*, 1340. [[CrossRef](#)] [[PubMed](#)]